Jour. Korean Earth Science Society, v. 23, no. 4, p. 357–368, April 2002

Dynamics of Barrel-Shaped Young Supernova Remnants

Hyun-Chul Jung[1,*] · Seung-Urn Choe[2]

[1]Center for Educational Research, Seoul National University, Seoul 151-742, Korea
[2]Department of Earth Science, Seoul National University, Seoul 151-742, Korea

항아리 형태 젊은 초신성 잔해의 동력학

정현철[1,*] · 최승언[2]

[1]서울대학교 교육종합연구원, 151-742 서울시 관악구 신림동 산 56-1
[2]서울대학교 지구과학교육과, 151-742 서울시 관악구 신림동 산 56-1

Abstract : In this study we have tried to explain the barrel-shaped morphology for young supernova remnants considering the dynamical effects of the ejecta. We consider the magnetic field amplification resulting from the Rayleigh-Taylor instability near the contact discontinuity. We can generate the synthetic radio image assuming the cosmic-ray pressure and calculate the azimuthal intensity ratio (A) to enable a quantitative comparison with observations. The postshock magnetic field are amplified by shearing, stretching, and compressing at the R-T finger boundary. The evolution of the instability strongly depends on the deceleration of the ejecta and the evolutionary stage of the remnant. The strength of the magnetic field increases in the initial phase and decreases after the reverse shock passes the constant density region of the ejecta. However, some memory of the earlier phases of amplification is retained in the interior even when the outer regions turn into a blast wave. The ratio of the averaged magnetic field strength at the equator to the one at the pole in the turbulent region can amount to 7.5 at the peak. The magnetic field amplification can make the large azimuthal intensity ratio (A = 15). The magnitude of the amplification is sensitive to numerical resolution. This means the magnetic field amplification can explain the barrel-shaped morphology of young supernova remnants without the dependence of the efficiency of the cosmic-ray acceleration on the magnetic field configuration. In order for this mechanism to be effective, the surrounding magnetic field must be well-ordered. The small number of barrel-shaped remnants may indicate that this condition rarely occurs.

Keywords : supernova remnant, magnetic field, cosmic ray, dynamics

요 약 : 본 연구에서는 항아리 형태 젊은 초신성 잔해의 동력학을 설명하기 위해 분출물의 동력학적 효과를 고려하였다. 분출물과 성간 물질 사이에 존재하는 접촉불연속면에서 레일라이-테일러(R-T) 불안정에 기인한 자기장의 증폭효과가 고려되었다. 우주선 입자의 가속을 가정함으로서 합성전파 모형을 만들 수 있었으며 관측과의 비교를 위해 방위각을 따른 전파세기의 비(A)를 계산하였다. R-T 불안정의 결과로 자란 가지의 경계면에서 압축, 전단, 인장의 결과로 충격파 후면의 자기장은 증폭되었다. 불안정의 시간에 따른 변화는 분출물의 감속에 민감하게 의존하며 초신성 잔해의 진화와 밀접히 관계됨을 볼 수 있었다. 자기장의 세기는 초기에 급격히 증가하며 역 충격파가 분출물의 등밀도지역으로 들어감에 따라 감소되었다. 그러나 이와 같은 초기 자기장 증폭의 효과는 초신성 잔해의 후기까지 남아 있음을 볼 수 있었다. 증폭된 자기장 영역에서 적도지역과 극지역의 자기장의 세기의 비는 최대 7.5까지 이를 수 있었다. 이와 같은 자기장의 증폭은 방위각에 따라 매우 큰 전파세기의 비를 만들 수 있었다(A = 15). 증폭된 자기장의 세기는 수치계산의 분해능에 매우 민감함을 알 수 있었다. 본 연구에서는 우주선 입자의 가속효과가 자기장과 충격파 면이 이루는 각도에 의존한다는 가정 없이도 자기장의 증폭효과가 관측된 항아리 형태의 젊은 초신성 잔해를 만들 수 있음을 보였다. 그러나 이와 같은 기작이 효과적이기 위해서는 초신성 잔해 주위의 자기장이 잘 정열되어 있어야 한다. 항아리 형태의 젊은 초신성 잔해의 수가 적게 관측되는 것은 이와 같은 조건이 성간에서 잘 이루어지지 않음을 의미한다.

주요어 : 초신성잔해, 자기장, 우주선, 동역학

*Corresponding author: jastro@korea.com

Introduction

After the highly energetic($\simeq 10^{51}$ ergs of kinetic energy) explosion of a supernova, the ejected material drives a blast wave into the ambient interstellar medium to produce a supernova remnant. As the supernova remnant shock wave sweeps up the ambient medium, the physical configuration and the morphology of the remnant can be strongly affected by the ambient medium.

Previous studies of the morphology of supernova remnants have simply classified these objects as either "shell-type" or "filled-center". The shell-type is characterized by a limb-brightened circularly symmetric appearance, consistent with a thin-walled spherical distribution of emissivity and is thought to be a natural outcome of a supernova explosion in a uniform medium, in the absence of a central pulsar. It has long been recognized that in few of the shell-types is the circular symmetry complete. Kesteven and Caswell (1987) found that some degree of bilateral symmetry can be discerned in the radio emission of more than 60% of Galactic remnants and suggested that the majority of shell-type supernova remnants could be bilateral, bipolar, axially symmetric, or, as we shall describe it, "barrel-shaped". There are three principal observational signs of the barrel-shaped supernova remnant morphology: (a) there is an axis of symmetry, (b) the shell has two regions of low intensity near the top and the bottom of the symmetry axis, and (c) there is a gradient of the radio brightness along the shell (Kesteven and Caswell, 1987; Roger *et al.*, 1988; Caswell *et al.*, 1992). Fig. 1 shows the radio maps of the typical supernova remnants (SN 1006) which demonstrate all features of barrel-shaped morphology: high degree of circular symmetry in radial outline and in radio emission (Reynolds and Gilmore, 1986).

It is generally accepted that the barrel-shaped supernova remnant represents an underlying cylindrical symmetry, the emitting regions corresponding to the curved walls of the cylinder. A barrel-

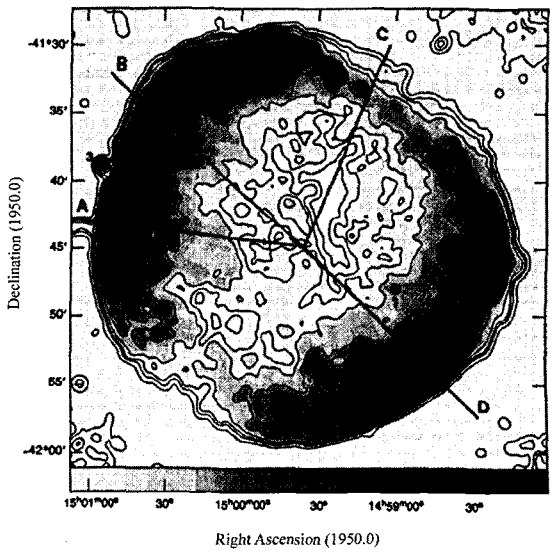

Fig. 1. Contour/grey scale plot of SN 1006 at the 1370 MHz (Reynolds and Gilmore, 1986).

shaped appearance is then produced when the barrel axis is approximately in the plane of the sky, the two bright flanks running parallel to this axis (Roger *et al.*, 1988). Various mechanisms, which might be responsible for the barrel-shaped appearance, have been suggested. These models may be broadly divided into three categories: (a) central pulsar model (Willingale *et al.*, 1996), (b) asymmetric density model (Bisnovatyi-kogan *et al.*, 1990), and (c) ambient magnetic field model (Van der Laan, 1962; Whiteoak and Gardner, 1968). It should be noted that it is possible that the different mechanism works at the different evolutionary stage and more than one of these mechanisms work simultaneously.

More recent high resolution observations of radio supernova remnants have revealed strong evidence that the axis of the symmetry of the barrel-shaped supernova remnants is aligned with Galactic plane, supposedly along the direction of the magnetic field (Gaensler, 1998). If the barrel-shaped remnants have the symmetric axis aligned with Galactic plane magnetic field, it means that the galactic magnetic field causes these supernova remnants to appear barrel-shaped. It has long been known that

the remnants in the adiabatic phase must exhibit the acceleration of energetic electrons and/or the amplification of magnetic field, since such remnants are far too bright in synchrotron radio emission for the emissivity to result from simply compressing ambient magnetic field and cosmic-ray electrons (Duin and Strom, 1975; Matsui *et al.*, 1984).

Fulbright and Reynolds (1990) generated model SNRs based on several classes of assumption regarding shock acceleration. In order to compare quantitatively the model supernova remnant with the observations, they used what they call as the "azimuthal intensity ratio", which is a ratio of the minimum to maximum intensity of emission along the shell. The azimuthal intensity ratio, A, is found by first determining the point at which the intensity of the shell is greatest. Along the circumference with the same radius, the minimum intensity is found and the ratio of maximum to minimum along this radius is A. They selected the 8 remnants which is believed to be in the adiabatic, Sedov phase and determined a value of the azimuthal intensity ratio by deducing it from the contour maps or grey scale images of the observed remnants. They concluded that the dependence of the efficiency of diffusive shock acceleration on the oblique angle θ_{Bn} between the shock normal and the ambient magnetic field must be considered for the barrel-shaped supernova remnants. They rely heavily on the work of Jokipii (1987). He has suggested that quasi-perpendicular "shock drift" acceleration takes place much more rapidly than quasi-parallel diffusive acceleration. However, the electrons we observe in radio supernova remnants have energies of typically 1-10 GeV, so low that they are essentially instantaneously accelerated, and difference in rates is unobservable (Voelk and Bierman, 1988; Ratkiewicz *et al.*, 1994).

Extensive polarization observations have showed that the projected mean magnetic fields tend to exhibit a cellular pattern with a net radial orientation for young supernova remnants while old remnants tend to exhibit a tangential mean magnetic field structure (Milne, 1987). It has been suggested that the contact interface between the ejecta and the shocked ambient medium is Rayleigh-Taylor unstable (Gull, 1973; Chevalier, 1976) due to the strong deceleration felt by the denser ejecta as it sweeps up lighter ambient gas. Gull (1973, 1975) suggested that the Rayleigh-Taylor instability in the decelerating stage (pre-Sedov stage) could amplify the magnetic field and make the field radial, which could explain the radio emission from the young supernova remnants.

In this study, we try to explain the barrel-shaped young supernova remnants with considering the dynamical effects of supernova remnants in the pre-Sedov stage on the distribution of radio emission. We will show that the magnetic field amplification through the Rayleigh-Taylor instability may explain the barrel-shaped morphology numerically. In §2 we present the methodology of our numerical calculations and model assumption. The results are described and analyzed in §3. Finally, discussions and conclusions are summarized in §4.

Numerical Method and Model Assumptions

In order to study the magnetic field amplification in Type Ia supernova remnant, we use the MHD ZEUS-3D. This is the three-dimensional extension of ZEUS-2D, fully described in Stone and Norman (1992). ZEUS-3D is an explicit, Eulerian code that integrates the ideal MHD equations in the absence of viscosity and diffusivity. Shock is treated using von Neumann-Rychtmeyer artificial viscosity. Fluid is advected through the mesh using the upwind, monotonic interpolation scheme of van Leer advection. Magnetic fields are transported using the constrained transport method (Evans and Hawley, 1988) modified with the method of characteristics to treat Alfven waves. Although ZEUS-3D is fully three-dimensional, it works efficiently in one or two dimensions (Jun, *et al.*, 1996).

When the shock wave from the explosion reaches the surface of the progenitor, the expanding ejecta develops a constant density core and an envelop with a steep power-law density gradient $\rho \propto \gamma^{-n}$. Type Ia SNs were modeled with $n = 7$ (Colgate and Mckee, 1969). Chevalier (1982) developed a self-similar solution for the adiabatic expansion of a stellar envelop with a steep power-law density gradient into a stationary ambient medium. As an initial condition the power-law envelope is extended to a radius close to the radius predicted by Chevalier' solution (Chevalier, 1982; Choe and Jung, 1998). The background density is chosen to be uniform with $n_0 = 1\ cm^{-3}$. The background magnetic field is chosen to be 5 μG and also assumed to be uniform. Many observational studies of the interstellar magnetic field have been made using pulsar dispersion and rotation measure or Zeeman effect measurements in HI at 21 cm. Rand and Kulkarni (1989) using rotation and dispersion measures from 116 pulsars found the rms strength of the magnetic field to be approximately 5 μG. While observational data on length scales of 1~10 pc are scarce, the galactic field is not expected to show strong variations on these scales (Heiles, 1976). This is likely in the environment of Type Ia.

We used spherical polar coordinate and calculated the flow only in one spherical quadrant. We used reflection symmetry on the equator and axis, and continuous on the outer boundary. To study the instability we need the initial seed perturbation. The scale of the initial perturbation for the instability was 2% in density. Only 3 cells inside contact discontinuity were randomly perturbed. The initial growth of the instability is very sensitive to the initial perturbation amplitude. However, once the instability entered the nonlinear regime, the initial

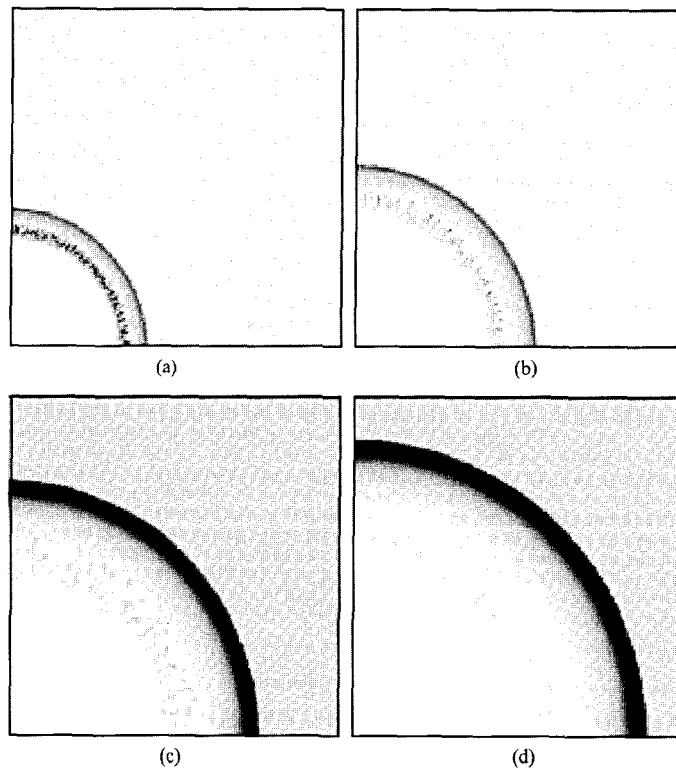

Fig. 2-a. Grey scale images of the density at 300 (a), 500 (b), 1,000 (c), 1400 (d) years. The dark region corresponds to maximum value.

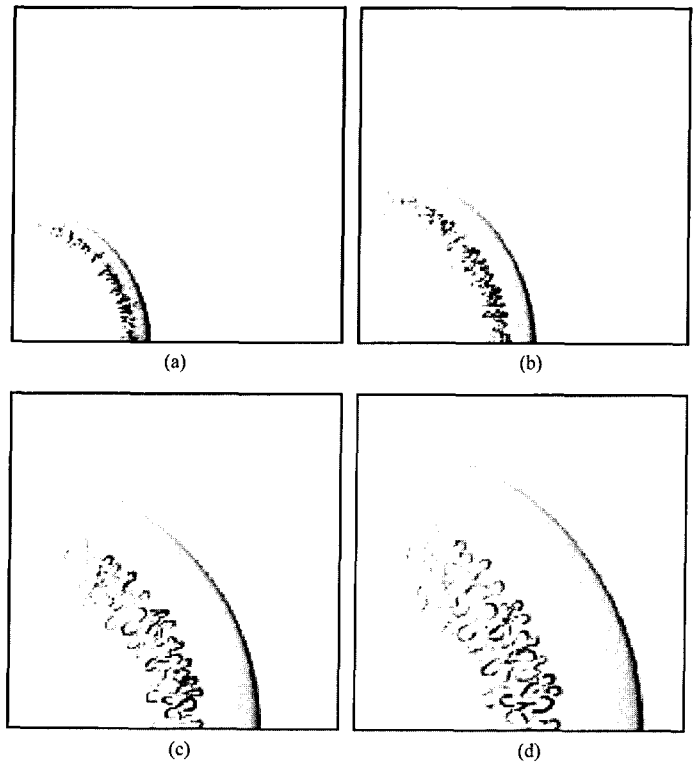

Fig. 2-b. Same as Fig. 2-a, for the magnetic pressure. The dark region corresponds to maximum value.

perturbation do not affect the final state. We started the simulation at r = 0.5 pc. Although this value is larger than the stellar radius of the presupernova, the important variable in the evolution is the mass ratio rather than the initial radius (Choe and Jung, 1998). To study the effects of the numerical resolutions, we ran three cases: (high: 600×400, medium: 300×200, low: 150×100).

Results

Evolution of the instabilities

The initial interaction of the ejecta with the ambient medium can create gradient of opposite sign in density and pressure near the contact discontinuity. Such a condition is sufficient for the formation of Rayleigh-Taylor instabilities (Jones *et al.*, 1981).

Fig. 2-a, b show grey scale images of density and magnetic pressure at t = 300, 500, 1,000, 1,400 years. By 300 years the reverse shock penetrates the constant density region of the ejecta, the density of the unshocked ejecta impinging on the interaction region decreases, the force of the "piston" lessens, and the expansion slows. The reverse shock approaches the center and the supernova remnant evolves into the Sedov stage at 1,400 years.

At early time the short wavelengths appear first because the growth rate is inversely proportional to the square root of the wavelength. As the finger moves away from the denser shell, the motion of the finger through the high-entropy region is inhibited by the drag on the head of the finger. The relative flow between a finger and its surroundings generates the Kelvin-Helmholtz instabilities that kink the stem and disrupt the flow through the finger and make the mushroom cap in the tip of the finger. The Kelvin-Helmholtz instabilities on the side of the finger can even detach the finger.

Because of flux freezing, the magnetic fields are amplified by shearing, stretching, and compression at the finger boundary.

At later time the finger growth is suppressed by the divergence of the volume in spherical coordinates decreasing the density contrast between the finger material and the postshock gas, by weakening of the deceleration, and by the ram pressure due to negative velocity gradient in decelerating stage. We can see the basic structures of a supernova remnant shell : undisturbed ambient gas, forward shock, shocked ambient gas, turbulent mixing layer, reverse shock and unshocked stellar ejecta. Weak magnetic fields have no effects on the growth rate of the instability dynamically. We can see the large finger at the later stage, partially by overtaking the small structures. High magnetic pressure is found around the tip of the finger and the bubble. Magnetic pressure at the tip of the fingers is greater than that at the bubbles, since the fingers have larger terminal velocity than the bubbles.

To study the evolution of both fluid and magnetic fields through the instability, the time history of the peculiar kinetic energy density and the peculiar magnetic energy density is shown in Fig. 3. Due to the expansion of supernova remnant, the dependence of the structure and the strength of the shocked magnetic field on the polar angle, it is very difficult to define the peculiar components which came from the instabilities only. So we ran another simulation without the instability. Then peculiar kinetic and magnetic densities are calculated by the excluding values without the instability from ones with the instability. This definition gives us accumulated peculiar energy densities. We can see that the above definition traced well out the peculiar components. The contribution from the other region is less than 0.01%.

Peculiar energy densities grow rapidly at first due to the rapid growth of the Rayleigh-Taylor instability during the initial strong deceleration phase. We can see that the radial component is dominant in

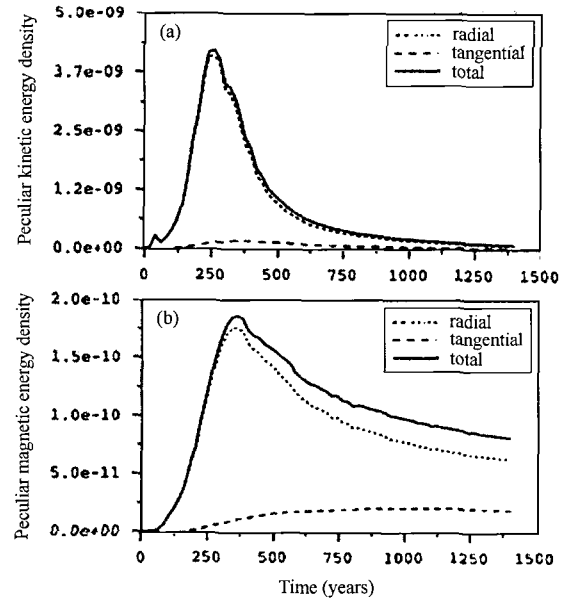

Fig. 3. Evolution of the peculiar energy densities (a) kinetic energy density (b) magnetic energy density. See the text for the definition of the peculiar energy density.

the initial phase. As the finger moves into the high-entropy region, the Kelvin-Helmholtz instability gives more tangential components relative to the radial components. After the first rapid rise, both peculiar energy densities decrease dramatically due to the weak deceleration (energy source for the instability) and the expansion. The radial component of magnetic field also dominates initially. This dominance is attributed to main amplification mechanism by stretching of the field line. At the peak, the peculiar magnetic energy density is only 4.25% of peculiar kinetic energy density. The calculated energy partition within the model supernova remnant are displayed the increase in the magnetic energy by the instabilities, though small amount.

Angle dependence

For the adiabatic shock the component of magnetic field perpendicular to the shock direction is amplified by the compression factor, which is 4, but the radial component is left unchanged. The magnitude of shocked ambient magnetic field at

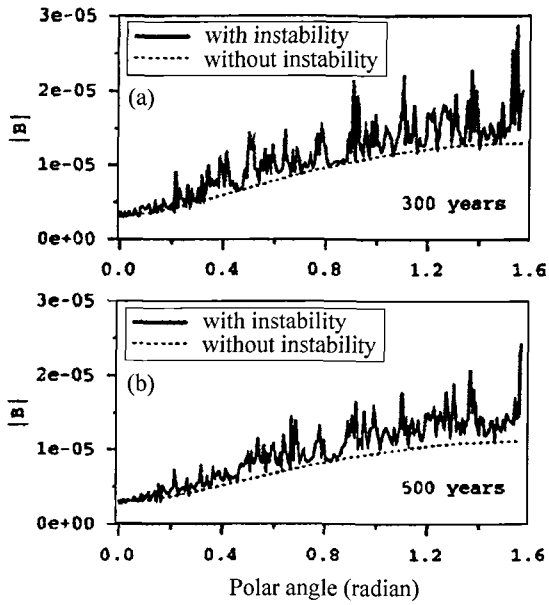

Fig. 4. Angle dependence of the amplified magnetic field strength resulting from Rayleigh-Taylor instability at 300 (a), 500 (b) years. For comparison, the case without the instability was displayed.

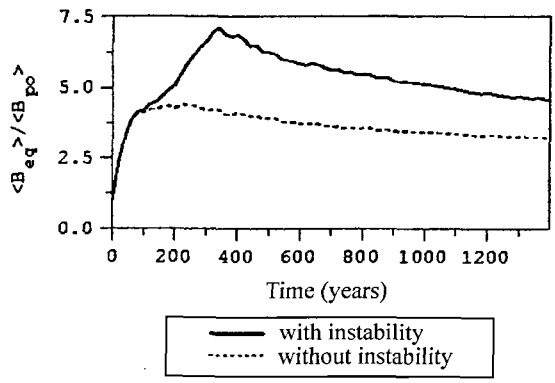

Fig. 5. Variation of the ratio of the magnetic field at the equator to the one at the pole for cases with/without the instability.

the equator is larger than the one at the pole by a factor of 4. We expect that the amplification of the magnetic field is a monotonic function of the initial magnetic field. However, the structure of the amplified magnetic field is not easy to describe because it varies significantly with time and with the polar angle. We have plotted the averaged magnetic field at 300 years and 500 years in Fig. 4. The magnetic field is averaged from innermost bubble to outermost bubble along the each ray. The Rayleigh-Taylor instability leads to many bumps and wiggles, but the magnitude of magnetic field tends to hover around a well-defined value. For comparison, we have plotted the magnitude of magnetic field expected without the instability. The local magnetic field strength at the equator increases over 30 times. High magnetic pressure is found around the tip of the finger and the bubble. At late time, the strength of the field decreases. The strong variations over time are attributes to the growth and decay of Rayleigh-Taylor fingers emanating from the shell of shocked ejecta. Fig. 5 shows the evolution of the ratio of the magnetic field pressure at the equator to the one at the pole. After 300 yrs, when the reverse shock penetrates the constant density region of the ejecta, the strength of the magnetic field in the turbulent region decreases under the values at the postshock region by the expansion. So the azimuthal intensity ratio approaches the one without the instability.

Radio emission

We assume that the radio emission is due to non-thermal synchrotron radiation. Since we are not modeling the acceleration and the transport of relativistic electrons, we need to assume the cosmic-ray pressure with the fluid variables. It was assumed that the pressure of cosmic ray is proportional to the postshock pressure and the electron acceleration efficiency does not change with time. This assumption requires that electron diffusion lengths be short enough to confine relativistic electrons to the same fluid element. We see this by considering the rate at which the relativistic electrons diffuse. The diffusion coefficient is written as $x \simeq cL_c$ if L_c is some characteristic length scale (Reynolds and Chevalier, 1981) and c is light speed. For diffusion in a peculiar field, with scale size λ_t(= 0.1 pc), L_c has been estimated variously as r_L(the Larmor radius), $(r_L \lambda_t)^{1/2}$, or r_L^2/λ_t. The distance a particle diffuses in time t is $x \simeq (L_c ct)^{1/2}$.

For any of these estimates of L_c, x ($<10^{13}$ cm) is generally small compared with the remnant size or the grid size used. Thus, we can ignore the diffusion of cosmic-ray through the background fluid.

We can calculate the synchrotron emissivity j_ν by the relation(Fulbright and Reynolds, 1990)

$$j_\nu = c_j K B_{\perp(s+1)/2}\, \nu^{(1-s)/2} \text{ ergss}^{-1}\text{ cm}^{-3}\text{ Hz}^{-1}\text{ sr}^{-1} \quad (1)$$

where c_j is a constant depending upon the value of s, $B_\perp$ is the component of magnetic field perpendicular to the line of sight, and K and s are related to the relativistic energy distribution by

$$N(E) = KE^{-s}\text{ cm}^{-3}\text{ ergs}^{-1}. \quad (2)$$

We expect that the emissivity strongly depends on the strength of the magnetic field. To generate the synthetic radio images, we assume the ϕ-symmetry. Because the synchrotron emissivity depends upon the component of the magnetic field perpendicular to the line of sight, as the inclination of the field external to the remnant is varied the synthetic radio map produced will also changed. When the external magnetic field is parallel to the observer's line of sight ($\theta_B = 0$), the remnant will be axially symmetry (A = 1). Grey scale synthetic radio images for inclination angle (θ_B) of 0° to 90° spaced every 30 DEG from the model remnant at 500 years are shown in Fig. 6. We can see that these images has the bipolarity with inclination angles from 30° to 90°.

We can calculate the azimuthal intensity ratio (A) from the model supernova remnant. Fig. 7 shows the variation of the azimuthal intensity ratio (A) with time. In the initial strong deceleration stage the ratio increases due to the difference of the strength of the magnetic fields resulting from the instability. Especially at the peak of the instability the values of the ratio can be over 10, which is observed in young supernova remnant. At late time, the strength of the magnetic field in the tur-

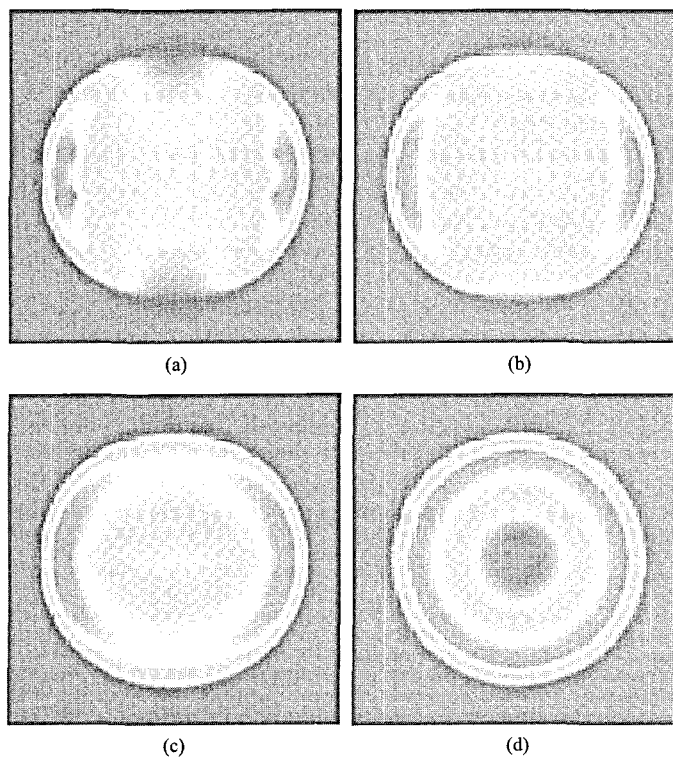

Fig. 6. Calculated synthetic radio images, (a) $\theta_B = 90°$, (b) $\theta_B = 60°$, (c) $\theta_B = 30°$, and (d) $\theta_B = 0°$.

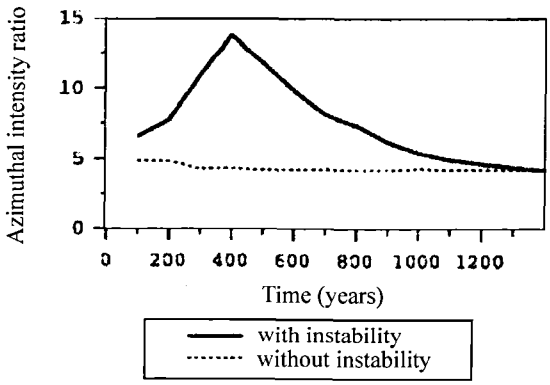

Fig. 7. Variation of the azimuthal intensity ratio (A) with time for cases with/without the instability.

bulent region decreases under the values at the postshock region by the expansion. So the azimuthal intensity ratio approaches the one without the instability.

Application to SN 1006

Our results can be applied to Type Ia supernova remnants. Unfortunately, we have only a few examples observed with high resolution (this is needed to decide the azimuthal intensity ratio, A). The most excellent example is SN 1006, which is regarded as the prototype for the barrel-shaped supernova remnants. The emission from SN 1006 shows pronounced bilateral symmetry both in outline and in emission intensity (Roger *et al.*, 1988). Measurements of the polarization have shown the emission regions of SN 1006 to have a radially aligned magnetic field components which is characteristic of young supernova remnants (Reynolds and Gilmore, 1993). The remnant outer edge is circular to within about 10% and the peak shell brightness varies by about a factor of 11 with azimuthal angle (Reynolds and Gilmore, 1986). We assume the number density of ambient gas to the value of 0.05 from the X-ray model (Hamilton *et al.*, 1986).

At 980 yrs, the calculated radius of the remnant is 6.9 pc, which gives the distance of 1.6 kpc. Swept-up mass is 2.46 $M_{\odot}$. The velocity of the

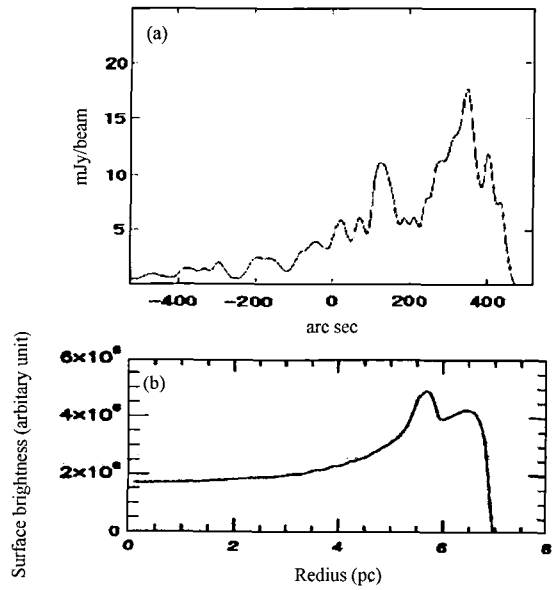

Fig. 8. (a) Slice b taken from Fig. 1 (Reynolds and Gilmore, 1986) (b) Calculated the radial profile of the surface brightness along the equator and the pole.

shock is 2,800km/sec. This value is in good agreement with that estimated by Kirshner *et al.* (1987). The data with which the numerical results are to be compared are contained in the radio map shown in Fig. 1. Slice b taken from the map are shown in Fig. 8-a. From the soft x-ray observation, the interstellar density in NW quadrant is a factor of 3 less than in the NE ans SW quadrants (Jones and Pye, 1989). Since we assumed the uniform ambient density, we are unable to compare the results completely. The radio intensity profile have two peaks. The outer peak of the intensity results from the shock and the inner peak of the intensity results from the Rayleigh-Taylor instability. Fig. 8-b shows calculated radio surface brightness along the equator and the pole. Table 1 shows the positions of the peaks from observation and calculation. The radio

Table 1. The position of the outer and inner peaks of the intensity.

	observation	model
R_{in}/R_s	0.87	0.83
R_{out}/R_s	0.94	0.93

shell extends inward 4 pc, depending upon where on the inner slope of the profile one chooses the edge. This result is in general agreement with the observations.

Discussion and Conclusions

In the reality the amplification of the magnetic field by turbulent dynamo can occur when the magnetic Reynolds number is sufficiently large so that the stretching of magnetic field lines may overcome Joule dissipation. And the magnetic field is not so strong as to prevent fluid motions, which amplify the field. Since we solve the ideal MHD equations, we ignore the magnetic diffusivity. However numerical diffusion works similarly to Joule dissipation and the grid resolution determines the level of dissipation. According to the study on the classical Rayleigh-Taylor instability, the peak of the magnetic energy spectrum occurs at the short wavelength (Jun *et al.*, 1995). It means the field is amplified preferentially on small scale. In numerical study, the smallest wavelength of the perturbation is decided as the numerical grid (angular grid). So we could expect that the higher resolution calculation would show the more magnetic energy and larger variation with the polar angle. In Fig. 9 we show the peculiar kinetic and magnetic energy densities with high resolution (600×400). The peculiar kinetic energy density increases by 2 times. On the contrary the peculiar magnetic energy density increases by four. The peculiar kinetic energy is decided by the large fingers because larger fingers have a higher terminal velocity. So they are less sensitive to the grid resolution. On the contrary the magnetic field strength in the mixing layer is found to increase with higher grid resolution because the effects of higher resolution is to decrease the numerical dissipation and enhance the peculiar amplification of the field.

Our magnetic field model can explain the large intensity ratio, circular morphology and the radial magnetic field structure. But the radial mean magnetic field appears to occur right at the shock front as well as interior to it, which can not explain by our model. If the supernova remnant expands into a clump (cloudy) circumstellar medium, the larger Rayleigh-Taylor finger can obtain a sufficient terminal velocity by taking extra kinetic energy from vortices generated by shock-cloud interactions (Jun *et al.*, 1996). The Rayleigh- Taylor finger can reach the forward shock front. The final field structure depends on the size, mass density, and distribution of clouds being engulfed by the supernova shock.

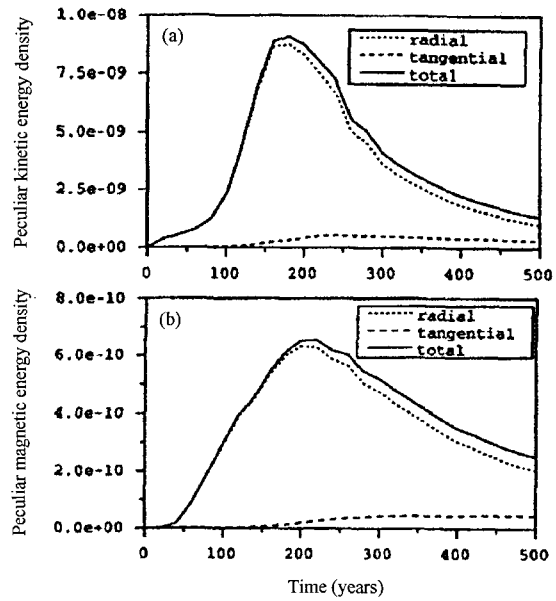

Fig. 9. Evolution of the peculiar energy densities (a) kinetic energy density (b) magnetic energy density. Compare with Fig. 3.

In this study we simply assumed that the pressure of cosmic ray is proportional to the postshock pressure. However, the dynamical feedback from the cosmic rays could be important and affect the pattern of the synchrotron emission (Jones and Kang, 1992). Ratkiewicz *et al.* (1994) showed that the effects of the dynamical feedback of the cosmic-ray pressure can make the barrel-shaped supernova remnant without the assumption of the magnetic field amplification. But they need almost 100% efficiency of the cosmic-ray acceleration to fit the observed azimuthal intensity ratio of the young

supernova remnants. It is difficult to accept in view of the general study of supernova remnants. Both of the magnetic field amplification and the dynamical feedback of the cosmic-ray pressure can easily enhance the azimuthal intensity ratio (A).

In this study, we have tried to explain the apparent barrel-shaped morphology for young supernova remnants considering the dynamical effects of the ejecta. During the early phase of supernova remnants the magnetic field amplification resulting from the Rayleigh-Taylor instability near the contact discontinuity can make the large azimuthal intensity ratio. The evolution of the instability strongly depends on the deceleration of the ejecta and the evolutionary stage of the remnant. The ratio of the averaged magnetic field strength at the equator to that at the pole in the turbulent region can amount to 7.5 at the peak. However, the resulting intensity ratio is at most 14. This is attributed to low filling factor of strong magnetic field. The magnitude of the amplification is sensitive to numerical resolution. After the peak, the strength of the magnetic field become weak in turbulent region by weak deceleration. In order for this mechanism to be effective, the surrounding magnetic field must be well-ordered. The small number of barrel-shaped remnants may indicate that this condition rarely occurs.

References

Bisnovatyi-kogan, G.S., Lozinskaya, T.A., and Silich, S.A., 1990, Barrel-like Supernova Remnants. Astrophysics and Space Science, 166, 277-287.

Caswell, J.K., Kesteven, M.J., Stewart, R.T., Milne, D.K., and Haynes, R.H., 1992, G308.8-0.1 - an unusual supernova remnant containing a short-period pulsar, PSR J1341-6220. Astrophysical Journal, 399, L151-153.

Chevalier, R.A., 1976, The hydrodynamics of Type II supernovae. Astrophysical Journal, 207, 872-887.

Chevalier, R.A., 1982, Self-similar solutions for the interaction of stellar ejecta with an external medium. Astrophysical Journal, 258, 790-797.

Choe, S.-U. and Jung, H.C., 1998, Dynamics of Type Ia SNRs with Different Density Distributions: From Ejects-Dominant to Sedov-Taylor Stages, Publications of The Korean Astronomical Society, 12(1), 135-147.

Colgate, S.A. and Mckee, C., 1969, Early Supernova Luminosity. Astrophysical Journal, 157, 623-634.

Duin, R.M. and Strom, R.G., 1975, A multifrequency study of the radio structure of 3C10, the remnant of Tycho's supernova. Astronomy and Astrophysics, 39, 33-42.

Evans, C.R. and Hawley, J.F., 1988, Simulation of magnetohydrodynamic flows - A constrained transport method. Astrophysical Journal, 332, 659-677.

Fulbright, M.S. and Reynolds, S.P., 1990, Bipolar supernova remnants and the obliquity dependence of shock acceleration. Astrophysical Journal, 357, 591-601.

Gaensler, B.M., 1998, The Nature of Bilateral Supernova Remnants. Astrophysical Journal, 493, 781-790.

Gull, S.F., 1973, A numerical model of the structure and evolution of young supernova remnants. Monthly Notices of the Royal Astronomical Society, 161, 47-60.

Gull, S.F., 1975, The X-ray, optical and radio properties of young supernova remnants. Monthly Notices of the Royal Astronomical Society, 171, 263-270.

Hamilton, A.J.S., Sarazin, C.L., and Szymkowiak, A.E., 1986, The X-ray spectrum of TYCHO. Astrophysical Journal, 300, 713-721.

Heiles, C., 1976, The interstellar magnetic field. Annual review of astronomy and astrophysics, 14, 1-22.

Jones, E.M., Smith, B.W., and Straka, W.C., 1981, Formation of supernova remnants - The pre-blast-wave phase. Astrophysical Journal, 249, 185-194.

Jones, L.R. and Pye, J.P., 1989, EXOSAT observations of the remnant of SN1006. MNRAS, 238, 567-585.

Jones, T.W., and Kang, H.S., 1992, Cosmic-ray-modified supernova remnant shocks. Astrophysical Journal, 396, 575-586.

Jokipii, J.R., 1987, Rate of energy gain and maximum energy in diffusive shock acceleration. Astrophysical Journal, 313, 842-846.

Jun, B.I., Norman, M.L., and Stone, J.M., 1995, A Numerical Study of Rayleigh-Taylor Instability in Magnetic Fluids. Astrophysical Journal, 453, 332-350.

Jun, B.I. and Norman, M.L., 1996, On the Origin of Strong Magnetic Fields in Young Supernova Remnants. Astrophysical Journal, 465, 800-811.

Jun, B.I., Jones, T.W., and Norman, M.L., 1996, Interaction of Rayleigh-Taylor Fingers and Circumstellar Cloudlets in Young Supernova Remnants. Astrophysical Journal, 468, L59-63.

Kesteven, M.J. and Caswell, J.L., 1987, Barrel-shaped supernova remnants. Astronomy and Astrophysics, 183, 118-128.

Kirshner, R.P., Winkler, P.F., and Chevalier, R.A., 1987, High-velocity emission in young supernova remnants: SN 1006 and SN 1572. Astrophysical Journal, 315, L135-139.

Matsui, Y., Long, K.S., Dickel, J.R., and Greisen, E.W., 1984, A detailed X-ray and radio comparison of Kepler's supernova remnant. Astrophysical Journal, 287, 295-306.

Milne, D.K., 1987, An atlas of supernova remnant magnetic fields. Australian Journal of physics, 40, 771-787.

Rand, R.J. and Kulkarni, S.R., 1989, The local Galactic magnetic field. Astrophysical Journal, 343, 760-772.

Ratkiewicz, R., Axford, W.I., and Mckenzie, J.F., 1994, Similarity solutions for synchrotron emission from a supernova blast wave. Astronomy and Astrophysics, 291, 935-942.

Reynolds, S.P. and Chevalier, R.A., 1981, Nonthermal Radiation from Supernova Remnants in the Adiabatic Stage of Evolution. Astrophysical Journal, 245, 912-920.

Reynolds, S.P. and Gilmore, D.M., 1986, Radio observations of the remnant of the supernova of A.D. 1006. I - Total intensity observations. Astronomical Journal, 92, 1138-1144.

Reynolds, S.P. and Gilmore, D.M., 1993, Radio observations of the remnant of the supernova of AD 1006. II - Polarization observations. Astronomical Journal, 106, 272-283.

Roger, R.S., Milne, D.K., Kesteven, M.J., Wellington, K.J., and Hayes, R.F., 1988, Symmetry of the radio emission from two high-latitude supernova remnants, G296.5 + 10.0 and G327.6 + 14.6 (SN 1006). Astrophysical Journal, 332, 940-953.

Stone, J.M. and Norman, M.L., 1992, ZEUS-2D: A Radiation Magnetohydrodynamics Code for Astrophysical Flows in Two Space Dimensions. II. The Magnetohydrodynamic Algorithms and Tests. Astrophysical Journal Supplement, 80, 791-805.

Van der Laan, H., 1962, Intense shell sources of radio emission. Monthly Notices of the Royal Astronomical Society, 124, 179-185.

Voelk, H.J. and Biermann, P.L., 1988, Maximum energy of cosmic-ray particles accelerated by supernova remnant shocks in stellar wind cavities. Astrophysical Journal, 333, L65-68.

Whiteoak, J.B. and Gadner, F.F., 1968, A Supernova Remnant in Centaurus. Astrophysical Journal, 154, 807-813.

Willingale, R., West., R.G., Pye, J.P., and Stewart, G.C., 1996, ROSAT PSPC observations of the remnant of SN 1006. Monthly Notices of the Royal Astronomical Society, 278, 749-762.

2001년 11월 9일 원고 접수
2002년 1월 16일 수정원고 접수
2002년 3월 23일 원고 채택